J|A|C|S
ARTICLES
Published on Web 01/24/2004

Efficiency of Various Lattices from Hard Ball to Soft Ball: Theoretical Study of Thermodynamic Properties of Dendrimer Liquid Crystal from Atomistic Simulation

Youyong Li, Shiang-Tai Lin, and William A. Goddard III*

Contribution from the Materials and Process Simulation Center (Mail code 139-74), Division of Chemistry and Chemical Engineering, California Institute of Technology, Pasadena, California 91125

Received September 19, 2003; E-mail: wag@wag.caltech.edu

Abstract: Self-assembled supramolecular organic liquid crystal structures at nanoscale have potential applications in molecular electronics, photonics, and porous nanomaterials. Most of these structures are formed by aggregation of soft spherical supramolecules, which have soft coronas and overlap each other in the packing process. Our main focus here is to study the possible packing mechanisms via molecular dynamics simulations at the atomistic level. We consider the relative stability of various lattices packed by the soft dendrimer balls, first synthesized and characterized by Percec et al. (*J. Am. Chem. Soc.* **1997**, *119*, 1539) with different packing methods. The dendrons, which form the soft dendrimer balls, have the character of a hard aromatic region from the point of the cone to the edge with C_{12} alkane "hair". After the dendrons pack into a sphere, the core of the sphere has the hard aromatic groups, while the surface is covered with the C_{12} alkane "hair". In our studies, we propose three ways to organize the hair on the balls, Smooth/Valentino balls, Sticky/Einstein balls, and Asymmetric/Punk balls, which lead to three different packing mechanisms, Slippery, Sticky, and Anisotropic, respectively. We carry out a series of molecular dynamics (MD) studies on three plausible crystal structures (A15, FCC, and BCC) as a function of density and analyze the MD based on the vibrational density of state (DoS) method to extract the enthalpy, entropy, and free energies of these systems. We find that anisotropic packed A15 is favored over FCC, BCC lattices. Our predicted X-ray intensities of the best structures are in excellent agreement with experiment. "Anisotropic ball packing" proposed here plays an intermediate role between the enthalpy-favored "disk packing" and entropy-favored "isotropic ball packing", which explains the phase transitions at different temperatures. Free energies of various lattices at different densities are essentially the same, indicating that the preferred lattice is not determined during the packing process. Both enthalpy and entropy decrease as the density increases. Free energy change with volume shows two stable phases: the condensed phase and the isolated micelle phase. The interactions between the soft dendrimer balls are found to be lattice dependent when described by a two-body potential because the soft ball self-adjusts its shape and interaction in different lattices. The shape of the free energy potential is similar to that of the "square shoulder potential". A model explaining the packing efficiency of ideal soft balls in various lattices is proposed in terms of geometrical consideration.

1. Introduction

The liquid crystal phase formed by self-assembled supramolecules with 3D nanoscale periodicity has been researched extensively[1−13] and has potential applications in molecular electronics,[2] photonics,[5] and porous nanomaterials.[6] In particular, Percec and co-workers have advanced a rational design and synthesized monodendrons that self-assemble through various molecular recognition mechanisms into rodlike,[14] cylindrical,[15] and spherical[16] supramolecular dendrimers, which self-organize into column lattice[15] or cubic lattice.[1,4,16,17] Wedge-shaped

(1) Ungar, G.; Liu, Y.; Zeng, X.; Percec, V.; Cho, W. D. *Science* **2003**, *299*, 1208.
(2) Percec, V.; Glodde, M.; Bera, T. K.; Miura, Y.; Shiyanovskaya, I.; Singer, K. D.; Balagurusamy, V. S. K.; Heiney, P. A.; Schnell, I.; Rapp, A.; Spiess, H. W.; Hudson, S. D.; Duan, H. *Nature* **2002**, *419*, 384.
(3) Percec, V.; Ahn, C.-H.; Ungar, G.; Yeardley, D. J. P.; Moller, M.; Sheiko, S. S. *Nature* **1998**, *391*, 161.
(4) Hudson, S. D.; Jung, H.-T.; Percec, V.; Cho, W.-D.; Johansson, G.; Ungar, G.; Balagurusamy, V. S. K. *Science* **1997**, *278*, 449.
(5) Lopes, W. A.; Jaeger, H. M. *Nature* **2001**, *414*, 735.
(6) Attard, G. S.; Goltner, C. G.; Corker, J. M.; Henke, S.; Templer, R. H. *Angew. Chem., Int. Ed. Engl.* **1997**, *36*, 1315.
(7) Jenekhe, S. A.; Chen, X. L. *Science* **1999**, *283*, 372.
(8) Zubarev, E. R.; Pralle, M. U.; Li, L.; Stupp, S. I. *Science* **1999**, *283*, 523.
(9) Stupp, S. I.; Braun, P. V. *Science* **1997**, *277*, 1242.
(10) Stupp, S. I.; LeBonheur, V.; Walker, K.; Li, L. S.; Huggins, K. E.; Keser, M.; Amstutz, A. *Science* **1997**, *276*, 384.
(11) Orr, G. W.; Barbour, L. J.; Atwood, J. L. *Science* **1999**, *285*, 1049.
(12) Harada, A.; Kataoka, K. *Science* **1999**, *283*, 65.
(13) Muthukumar, M.; Ober, C. K.; Thomas, E. L. *Science* **1997**, *277*, 1225.
(14) Percec, V.; Chu, P.; Ungar, G.; Zhou, J. *J. Am. Chem. Soc.* **1995**, *117*, 11441.
(15) Percec, V.; Johansson, G.; Ungar, G.; Zhou, J. *J. Am. Chem. Soc.* **1996**, *118*, 9855.
(16) Balagurusamy, V. S. K.; Ungar, G.; Percec, V.; Johansson, G. *J. Am. Chem. Soc.* **1997**, *119*, 1539.
(17) Yeardley, D. J. P.; Ungar, G.; Percec, V.; Holerca, M. N.; Johansson, G. *J. Am. Chem. Soc.* **2000**, *122*, 1684.

10.1021/ja038617e CCC: $27.50

Scheme 1. R = $C_{12}H_{25}$; **I**, G2 (12G2-AG); **II**, G3 (12G3-AG); **III**, G4 (12G4-AG)[a]

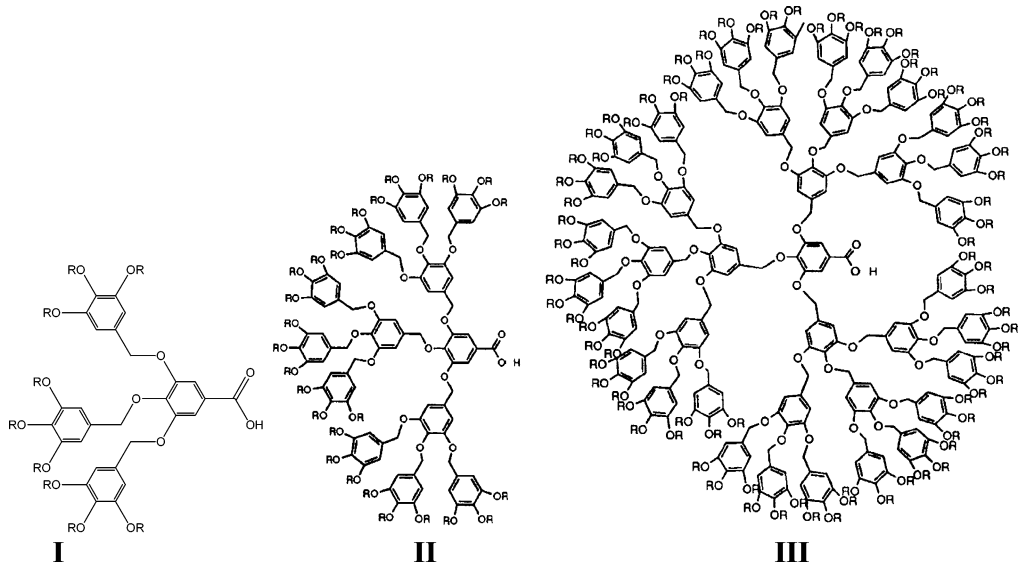

I **II** **III**

[a] We denote these as G2, G3, and G4 through the text. Illustrations of **II** and **III** are modified from reference 16. Reference 16 denotes them as 12G2-AG, 12G3-AG, and 12G4-AG, respectively, which are 12G2-AG, 3,4,5-tris[3′,4′,5′-tris(*n*-dodecan-1-yloxy)benzyloxy)]benzoic acid; 12G3-AG, 3,4,5-tris{3′,4′,5′-tris[3″,4″,5″-tris(*n*-dodecan-1-yloxybenzyloxy)benzyloxy]benzyloxy}benzoic acid; and 12G4-AG, 3,4,5-tris(3′,4′,5′-tris{3″,4″,5″-tris[3‴,4‴,5‴-tris(*n*-dodecan-1-yloxybenzyloxy)benzyloxy]benzyloxy}benzyloxy)benzoic acid.

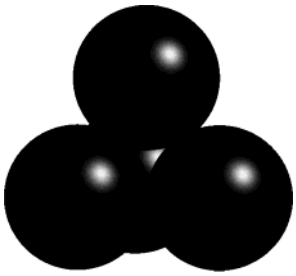

Figure 1. Close-packed hard balls.

dendrons such as **I**, **II**, and **III** depicted in Scheme 1 have so far been found to form either columnar or cubic phases. In the former, dendrons assemble flat pizza-like slices into disks, which then stack into columns, which eventually pack to form a hexagonal array.[15] Dendrons with more alkyl chains are cone-shaped and assemble into supramolecular spheres. So far, these spherical aggregates have been known to pack on three types of lattices, Cub $Pm\bar{3}n$,[16] Cub $Im\bar{3}m$,[17] and Tet $P4_2/mnm$.[1] The preferred formation of the $Pm\bar{3}n$ lattice in thermotropic spherodic cubic mesophases is a fact which surprises, especially as related ordered assemblies of block copolymers form the BCC ($Im\bar{3}m$) lattice. In addition, the $Pm\bar{3}n$ lattice was not only found for dendritic molecules, it was also reported for the thermotropic mesophases of amphiphilic molecules,[18,19] star-shaped molecules,[20] and amphiphiles with perfluorinated chains.[21]

One of the most important principles for packing hard spheres into periodic lattice is minimization of the interstitial volume (Figure 1), which leads to the face-centered cubic (cubic close-packed) structure and hexagonal close-packed structure. The packing of hard spheres (billiard balls and noble gases) into infinite two-dimensional arrays leads to close packing with each ball having six equally spaced neighbors in a plane with the planes packed into periodic arrays in three dimensions that lead to 12 nearest neighbors for each ball. Stacking the close-packed layers as ABCABC leads to the face-centered cubic (cubic close-packed, denoted FCC) structure, while ABABAB stacking of close-packed layers leads to the hexagonal close-packed structure (denoted HCP). Indeed, the stable crystal structure for all noble gases and the favored structures for most metals is FCC, HCP, or DHCP (hexagonal with ABACABAC packing). Another popular structure with metals is body-centered cubic (BCC) in which atoms are at the corners and center of a cube, leading to eight nearest neighbors. In addition, symmetric molecules such as CH_4 and C_{60} fullerene crystallize into structures that are slightly distorted FCC at low temperature and fully FCC at higher temperature. Furthermore, it has been shown that the face-centered cubic packing maximizes the total entropy.[22]

Obviously, the simple principles that explain the structure approproiate for hard balls such as noble gas atoms, CH_4, and C_{60} do not apply to soft spheres, which, instead of a simple ball−ball surface contact, have flexible hair that can overlap each other to achieve more complex packing as in Figure 2. Almost all self-assembled supramolecular aggregates are soft spheres and can be approximated by hard spherical cores and soft aliphatic coronas, as shown in Figure 2.

What would be the principle for packing soft balls together? Here, we propose three packing mechanisms of soft balls and use classical atomistic molecular dynamic simulations to investigate the efficiency of various lattices for soft balls from determining their thermodynamic properties. We focus on the three compounds **I**, **II**, and **III** (Scheme 1), which have been reported to form spheres with a nearly integer number of dendrons.[16] In section 2, we describe the details of our calculations. Section 3 reports the results and the discussion. The summary is presented in section 4.

(18) Borisch, K.; Diele, S.; Goring, P.; Tschierske, C. *Chem. Commun.* **1996**, *2*, 237.
(19) Borisch, K.; Diele, S.; Goring, P.; Muller, H.; Tschierske, C. *Liq. Cryst.* **1997**, *22*, 427.
(20) Cheng, X. H.; Diele, S.; Tschierske, C. *Angew. Chem., Int. Ed.* **2000**, *39*, 592.
(21) Cheng, X. H.; Das, M. K.; Diele, S.; Tschierske, C. *Langmuir* **2002**, *18*, 6521.
(22) Mau, S.-C.; Huse, D. A. *Phys. Rev. E* **1999**, *59*, 4396.

Table 1. Force Field Parameters Used for Coarse-Grained Alkane Segments; The Functional Forms Are Given in Eq 1[a,b] (All Parameters Are from the SKS United Atom Force Field Unless Otherwise Indicated)

$$E_{\mathrm{VDW}}(R) = D_0\left\{\left(\frac{R_0}{R}\right)^{12} - 2\left(\frac{R_0}{R}\right)^{6}\right\} \quad (1a)$$

$$E_{\mathrm{bond}}(R)^a = \frac{1}{2}K_R(R - R_0)^2 \quad (1b)$$

$$E_{\mathrm{angle}}(\theta) = \frac{1}{2}K_\theta(\theta - \theta_0)^2 \quad (1c)$$

$$E_{\mathrm{torsion}}(\phi)^b = \sum_n \frac{1}{2}V_n[1 - d_n\cos(n\phi)] \quad (1d)$$

E_{vdW}	CH_2	$R_0{}^c$	4.4113	$D_0{}^d$	0.09339		
	CH_3	$R_0{}^c$	4.4113	$D_0{}^d$	0.2265		
E_{bond}	CH_2-CH_2	$R_0{}^c$	1.54	$K_b{}^e$	520		
	CH_2-CH_3	$R_0{}^c$	1.54	$K_b{}^e$	520		
E_{angle}	$CH_2-CH_2-CH_2$	$\theta_0{}^f$	114	$K_\theta{}^g$	124.19		
	$CH_2-CH_2-CH_3$	$\theta_0{}^f$	114	$K_\theta{}^g$	124.19		
E_{torsion}	$CH_2-CH_2-CH_2-CH_2$	$V_1(d_1)^d$	1.4109(−1)	$V_2(d_2)^d$	−0.271(1)	$V_3(d_3)^d$	2.787(−1)
	$CH_2-CH_2-CH_2-CH_3$	$V_1(d_1)^d$	1.4109(−1)	$V_2(d_2)^d$	−0.271(1)	$V_3(d_3)^d$	2.787(−1)

[a] The force constants for the bond-stretching potential function were introduced from the AMBER force field[26,27] because the original SKS force field uses a fixed bond distance. [b] The torsion potential of the SKS force field had been taken from the OPLS (optimized potentials for liquid simulation) force field.[28] [c] In Å. For vdW, SKS uses $E_{\mathrm{VDW}}(R) = 4\epsilon\{(\sigma/R)^{12} - (\sigma/R)^6\}$. Thus, $R_0 = (2\sigma)^{1/6}$. [d] In kcal/mol. For vdW, D_0(kcal/mol) = $k\epsilon$(SKS), where k is the Boltzmann constant. [e] In kcal/(mol Å^2). [f] In degrees. [g] In kcal/(mol rad^2).

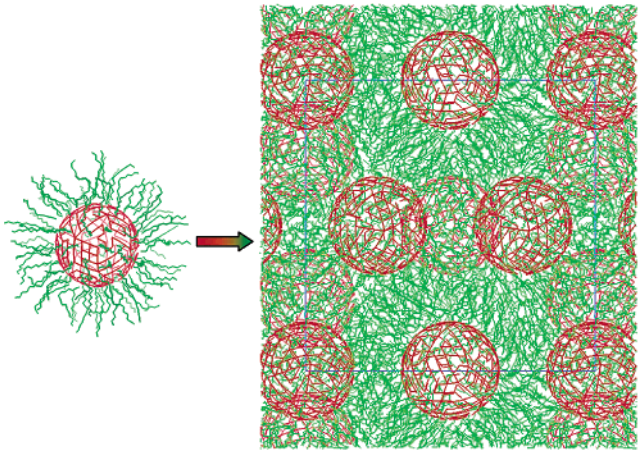

Figure 2. Overlapping packed soft balls.

2. Methods

2.1. Force Field. The methylene (CH_2) and methyl (CH_3) groups in $C_{12}H_{25}$ were treated as united atoms C_32 and C_33; that is, each CH_2 or CH_3 unit was treated as a single neutral pseudoatom. The van der Waals interaction for this coarse-grained polyethylene model is taken from the SKS (Siepmann−Karanorni−Smit) force field,[23−25] which was developed to describe the thermodynamic properties of *n*-alkanes. The bond-stretching force constant, which is not presented in the original SKS force field, is taken from the AMBER force field.[26,27] The torsion potential of the SKS force field had been taken from the OPLS (optimized potentials for liquid simulation) force field of Jorgensen.[28] The parameters for all other atoms including hybrid terms with C_32, C_33 are taken from the generic Dreiding force field.[29] There is no coulomb term in the setup energy of the simulation.

The force field for the coarse-grained polyethylene model uses valence terms of the form as shown in eq 1, with the parameters summarized in Table 1.

2.2. The Vibrational Density of States (DoS) from the Velocity Autocorrelation (VAC) Function. To obtain the vibrational density of states (DoS) $S(\nu)$ as a function of the frequency ν for a given density and temperature, we start with the mass weighted velocity autocorrelation (VAC) function

$$C(t) = \sum_{i=1}^{N}\sum_{\alpha=1}^{3} m_i c_{i\alpha}(t) \quad (2)$$

where m_i is the mass of atom i, and $c_{i\alpha}(t)$ is the α component (α = x, y, and z) of the velocity autocorrelation of atom i

$$c_{i\alpha}(t) = \lim_{\tau\to\infty}\frac{\int_{-\tau}^{\tau} v_{i\alpha}(t'+t)v_{i\alpha}(t')\,dt'}{\int_{-\tau}^{\tau} dt'} = \lim_{\tau\to\infty}\frac{1}{2\tau}\int_{-\tau}^{\tau} v_{i\alpha}(t'+t)v_{i\alpha}(t')\,dt' \quad (3)$$

Taking the Fourier transform of $C(t)$ then leads to the vibrational density of states (DoS)

$$S(\nu) = \frac{2}{kT}\lim_{\tau\to\infty}\int_{-\tau}^{\tau} C(t)\exp(-i2\pi\nu t)\,dt \quad (4)$$

Integrating $S(\nu)$ gives the total degrees of freedom of the system, that is,

$$\int_0^\infty S(\nu)\,d\nu = 3N \quad (5)$$

Generally, MD simulations for a condensed system remove the center of mass translations (3 degrees of freedom) because the energy must be independent of the origin. Thus, $S(\nu)$ is renormalized such that the integration of eq 5 gives 3N − 3.

From various test calculations, we found that recording the velocities every 4 fs is sufficient to obtain an accurate description of the high frequency DoS, and we found that a total time span (after equilibration) of 20−40 ps is generally adequate to give the low frequency modes sufficient for accurate entropies (see section 2.5).

2.3. Thermodynamic Properties from Molecular Dynamics. Given the vibrational density of states for a given V and T, we can calculate

(23) Siepmann, J. I.; Karaborni, S.; Smit, B. *Nature* **1993**, *365*, 330.
(24) Smit, B.; Karaborni, S.; Siepmann, J. I. *J. Chem. Phys.* **1995**, *102*, 2126.
(25) Martin, M. G.; Siepmann, J. I. *J. Am. Chem. Soc.* **1997**, *119*, 8921.
(26) Weiner, S. J.; Kollman, P. A.; Case, D. A.; Singh, U. C.; Ghio, C.; Alagona, G.; Profeta, S.; Weiner, P. *J. Am. Chem. Soc.* **1984**, *106*, 765.
(27) Weiner, S. J.; Kollman, P. A.; Nguyen, D. T.; Case, D. A. *J. Comput. Chem.* **1986**, *7*, 230.
(28) Jorgensen, W. L.; Madura, J. D.; Swenson, C. J. *J. Am. Chem. Soc.* **1984**, *106*, 6638.
(29) Mayo, S. L.; Olafson, B. D.; Goddard, W. A. *J. Phys. Chem.* **1990**, *94*, 8897.

the partition function $Q(V,T)$ by treating the continuous DoS as a continuum of uncorrelated harmonic oscillators

$$\ln Q = \int_0^\infty \mathrm{d}\nu\, S(\nu) \ln q_{\mathrm{HO}}(\nu) \tag{6}$$

where

$$q_{\mathrm{HO}}(\nu) = \frac{\exp(-\beta h\nu/2)}{1 - \exp(-\beta h\nu/2)} \tag{7}$$

is the partition function of a harmonic oscillator with vibrational frequency ν. Here, $\beta = 1/kT$, h is Planck's constant, and $S(\nu)\,\mathrm{d}\nu$ is the number of modes between frequencies ν and $\nu + \mathrm{d}\nu$. Given the partition function, the thermodynamic properties are determined as

$$E = V_0 + T\beta^{-1}\left(\frac{\partial \ln Q}{\partial T}\right)_{N,V} = V_0 + \beta^{-1}\int_0^\infty \mathrm{d}\nu\, S(\nu) W_E(\nu) \tag{8a}$$

$$S = k \ln Q + \beta^{-1}\left(\frac{\partial \ln Q}{\partial T}\right)_{N,V} = k\int_0^\infty \mathrm{d}\nu\, S(\nu) W_S(\nu) \tag{8b}$$

$$A = V_0 - \beta^{-1} \ln Q = V_0 + \beta^{-1}\int_0^\infty \mathrm{d}\nu\, S(\nu) W_A(\nu) \tag{8c}$$

where

$$W_E(\nu) = \frac{\beta h\nu}{2} + \frac{\beta h\nu}{\exp(\beta h\nu) - 1} \tag{9a}$$

$$W_S(\nu) = \frac{\beta h\nu}{\exp(\beta h\nu) - 1} - \ln[1 - \exp(-\beta h\nu)] \tag{9b}$$

$$W_A(\nu) = \ln\frac{1 - \exp(\beta h\nu)}{\exp(-\beta h\nu/2)} \tag{9c}$$

are weighting functions and V_o is a reference energy. Therefore, within the assumption that the system is ergotic within the time scale of the calculation, all thermodynamic properties are determined. We need to provide only the reference energy V_o and the vibrational density of states distribution $S(\nu)$ from the molecular dynamics simulations.

We choose the reference energy such that in the classical limit ($h \rightarrow 0$), the energy evaluated from eq 8a is equivalent to the total energy E_{MD} (kinetic plus potential) obtained from molecular dynamics simulation. For a system of harmonic oscillators in the classical limit, the energy is $3NkT$ (the equipartition theorem), where $3N$ is the total degrees of freedom of the system. Thus, we write the reference energy as

$$V_o = E_{\mathrm{MD}} - \beta^{-1} 3N \tag{10}$$

where N is the total number of atoms in the system. For condensed systems, the total degrees of freedom of the system are $3N - 3$, and eq 10 becomes $V_o = E_{\mathrm{MD}} - \beta^{-1}(3N - 3)$. It is useful to note that the energy (and free energy) determined this way includes the zero point energy (first term on the RHS of eq 9a). This contribution is important when quantum effects are significant in the system.

2.4. Molecular Dynamics Simulation. Molecular dynamics software Lammps[30] is used to perform NVT molecular dynamics simulations with the time step set to 1 fs. For each structure, we start by assigning the initial velocities (Gaussian distribution) on each atom to give a system temperature of 20 K, and then perform MD simulations for 10 ps at 10 K to equilibrate the structure. The temperature of the system is then increased from 10 to 277 K (recrystallization temperature) steadily over a period of 2 ps (the temperature was increased by 267/2000 K every time step), followed by equilibration runs at 277 K for 8 ps. A 40 ps NVT molecular dynamics is then performed with the atomic velocities, system energy, temperature, and pressure recorded every 4 fs. This trajectory information is later used in the velocity autocorrelation analysis to obtain the vibrational spectrum from which the thermodynamic properties were calculated. The use of 40 ps is found to be sufficient for obtaining a converged free energy as shown in section 2.5.

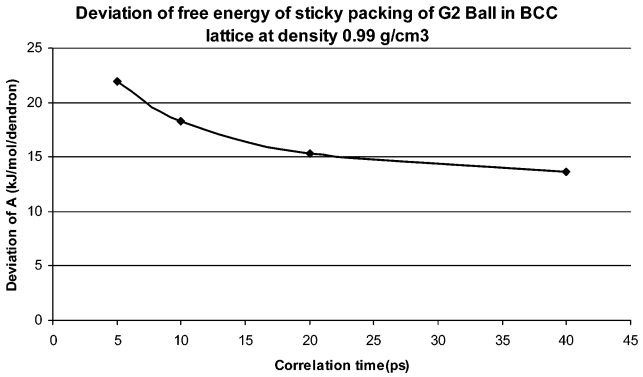

Figure 3. Convergence of the free energy from VAC.

Molecular dynamics are performed on a Linux cluster of 80 dual-processor Dell PowerEdge 2650s (P4 Xeon 2.2/2.4GHz, 2G Memory, 54G HD) at MSC. Each dynamics takes 1−5 days depending on the system size (4000−25 000 atoms).

2.5. Convergence of the Free Energy Calculation. To compare the efficiency of various lattices for dendrimer balls consistently, we build various lattice structures from the same initial isolated dendrimer ball (see section 3.3 below). However, there may exist deviations in the free energy evaluated from the molecular dynamics, especially for the entropy that is dominated by the low-frequency modes in the system. To access the convergence of our calculated thermodynamic properties, we run three independent molecular dynamics from the same initial structure but assign different initial velocity distributions (same overall system temperature). From the three different MD trajectories, we determine the RMS deviation of free energy, enthalpy, and entropy as shown in Figure 7 of section 3.4. To discuss how the deviation depends on the correlation time, we select the point with a large deviation in Figure 7A (sticky G2 Ball in BCC lattice) and calculate the deviations in free energy using different correlation times: 5, 10, 20, and 40 ps. Figure 3 shows that using a longer correlation time leads to a better free energy evaluation and 40 ps is sufficient to give satisfying deviation to compare various lattices as shown in Figure 7.

3. Results and Discussion

3.1. Three Proposed Packing Mechanisms of the Soft Balls with Polyethylene Tails. The liquid crystal phase formed by self-assembled supramolecules with 3D nanoscale periodicity has been researched extensively.[1−13] For example, studies of electron density profiles and histograms computed from the X-ray diffraction data[16] demonstrate that compounds **I**, **II**, and **III** are self-assembled in supramolecular dendrimers resembling spherical micelles, which self-organize in a three-dimensional cubic $Pm\bar{3}n$ lattice. This thermotropic liquid crystal phase is similar to that of the lyotropic $Pm\bar{3}n$ phase found in some amphiphile/water systems. These supramolecular dendrimers contain a poly(benzyl ether) core dispersed in an aliphatic matrix of nearly uniform density, which is made up of the melted terminal long alkyl chains of the monodendrons.

Geometrical aspects of liquid crystal phases have been studied in considerable detail for lyotropic systems[31−33] with interfacial

(30) *Large-Scale Atomic/Molecular Maasively Parallel Simulator, version 5.0*; CRADA collaboration, Sandia National Laboratory, USA, 1997.

(31) Sadoc, J. F.; Charvolin, J. *J. Phys. France* **1986**, *47*, 683.
(32) Israelachvili, J. *Intermolecular and Surface Forces*, 2nd ed.; Academic Press: London, 1992.

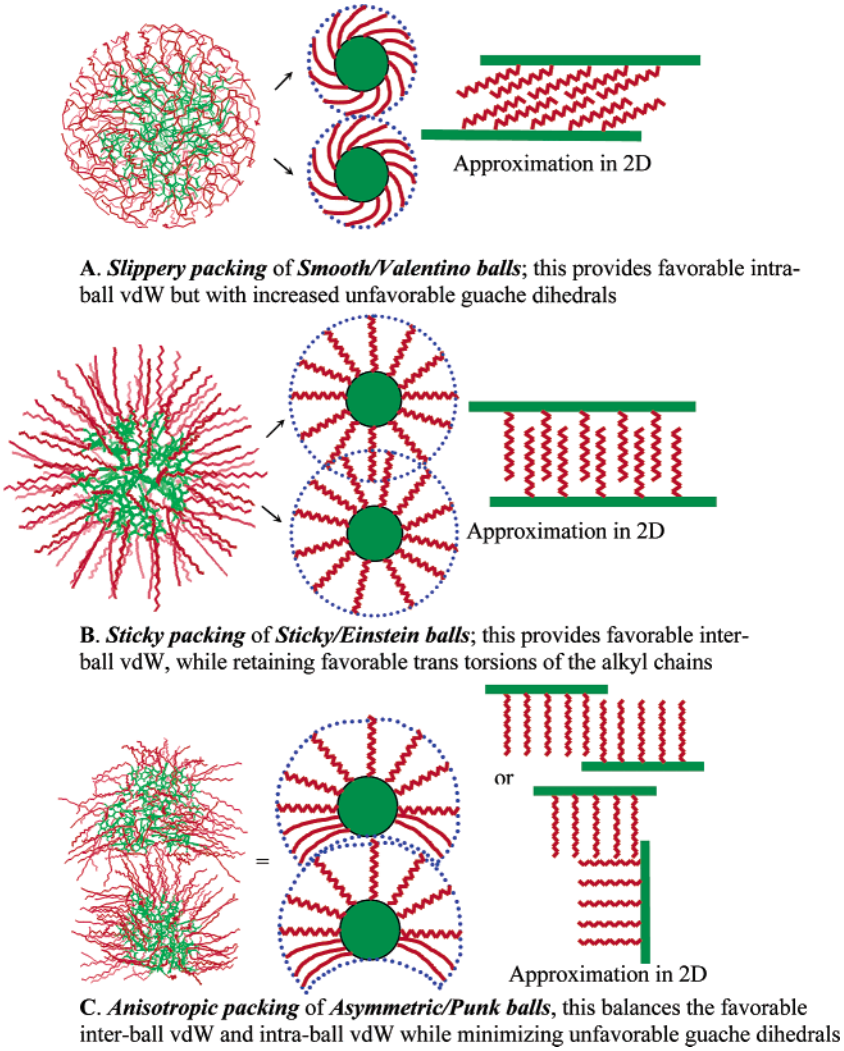

Figure 4. Three proposed packing mechanisms of soft balls with soft coronas composed of polyethylene chains.

curvature being recognized as the key factor for determining the phase type.[34,35] However, it is very difficult to investigate the interfacial curvature from experiment because of the nearly uniform density of the aliphatic matrix.

On the basis of our simulations on the atomistic scale, we propose three packing mechanisms of soft balls with soft coronas composed of polyethylene as shown in Figure 4.

For the soft balls having soft coronas composed of long alkyl chains, we considered three classes of structures:

Smooth/Valentino balls are shown in Figure 4A, which lead to the Slippery packing mechanism. Here, the C_{12} alkane "hair" is slicked down on each ball. This maximizes the favorable van der Waals attraction between intraball chains and is optimum for separate balls. However, the best intraball interactions may lead to an increase in the number of gauche dihedrals and hence less favorable torsional interactions. This likely leads to a minimum in the favorable interball interactions between the chains.

Sticky/Einstein balls are shown in Figure 4B, which lead to the Sticky packing mechanism. Here, the alkyl hairs stick out perpendicular to the surface to provide maximum surface area for adjacent balls to interact, maximizing the favorable intermolecular van der Waals attraction between chains of different balls. This likely leads to a minimum in the favorable intraball interactions between chains.

Asymmetric/Punk balls are shown in Figure 4C, which lead to the Anisotropic packing mechanism. Here, about half of the surface has Einstein type hair, and the other half has Valentino hair. This was motivated by the anisotropic positions on the faces of $Pm\bar{3}n$ lattice, where the balls have two close neighbor balls and other neighbor balls at a regular distance. In this packing mechanism, the core of the soft ball deforms to become nonspherical. The chains are slicked down (Valentino) to provide the most favorable by intraball VDW while accommodating the short distances between the closest balls on the faces, and they are extended (Einstein) to provide the best interball VDW with the other more distant neighbors. Thus, in this Anisotropic packing mechanism, the packing of polyethylene chains is a balance between the intraball type and the interball type. In this packing mechanism, the chain shape can be kept as nearly all-trans to minimize the torsional cost while optimizing the intraball and interball interactions.

3.2. Preparation of Dendrimer Balls of Different Shapes. We used Cerius2[36] to construct the three-dimensional structures

(33) Kratzat, K.; Finkelmann, H. J. *Colloid Interface Sci.* **1996**, *181*, 542.
(34) Gruner, S. M. *J. Phys. Chem.* **1989**, *93*, 7562.
(35) Tate, M. W.; Eikenberry, E. F.; Turner, D. C.; Shyamsunder, E.; Gruner, S. M. *Chem. Phys. Lipids* **1991**, *57*, 147.

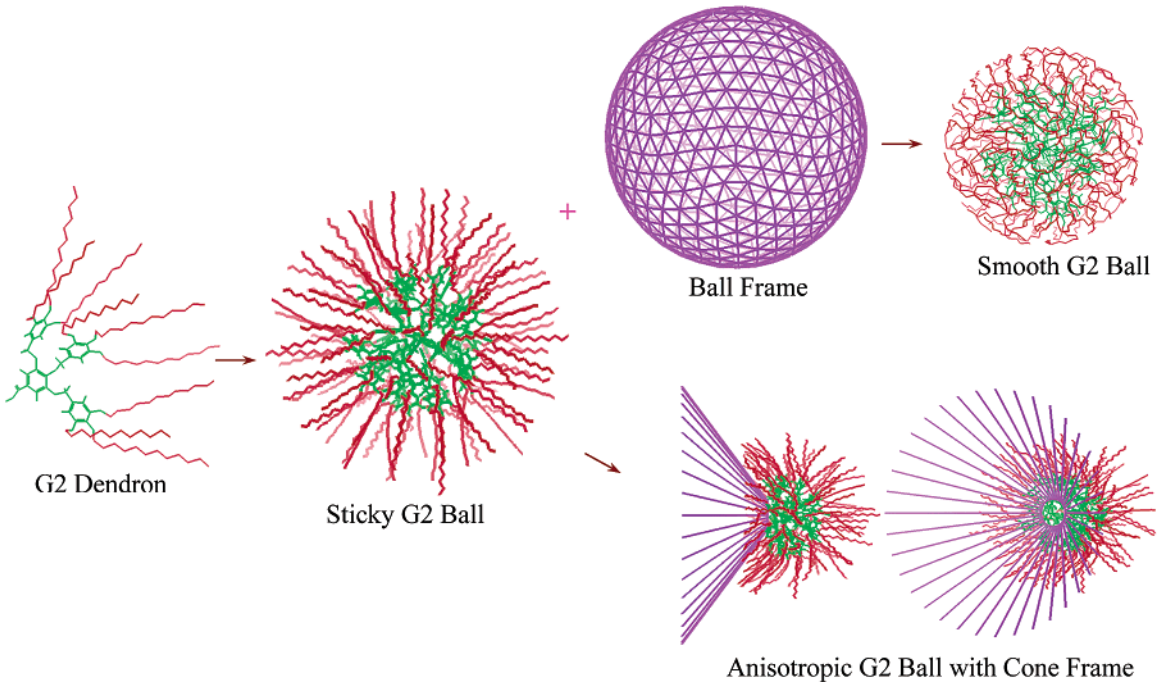

Figure 5. Preparation of the three shapes of G2 dendrimer ball.

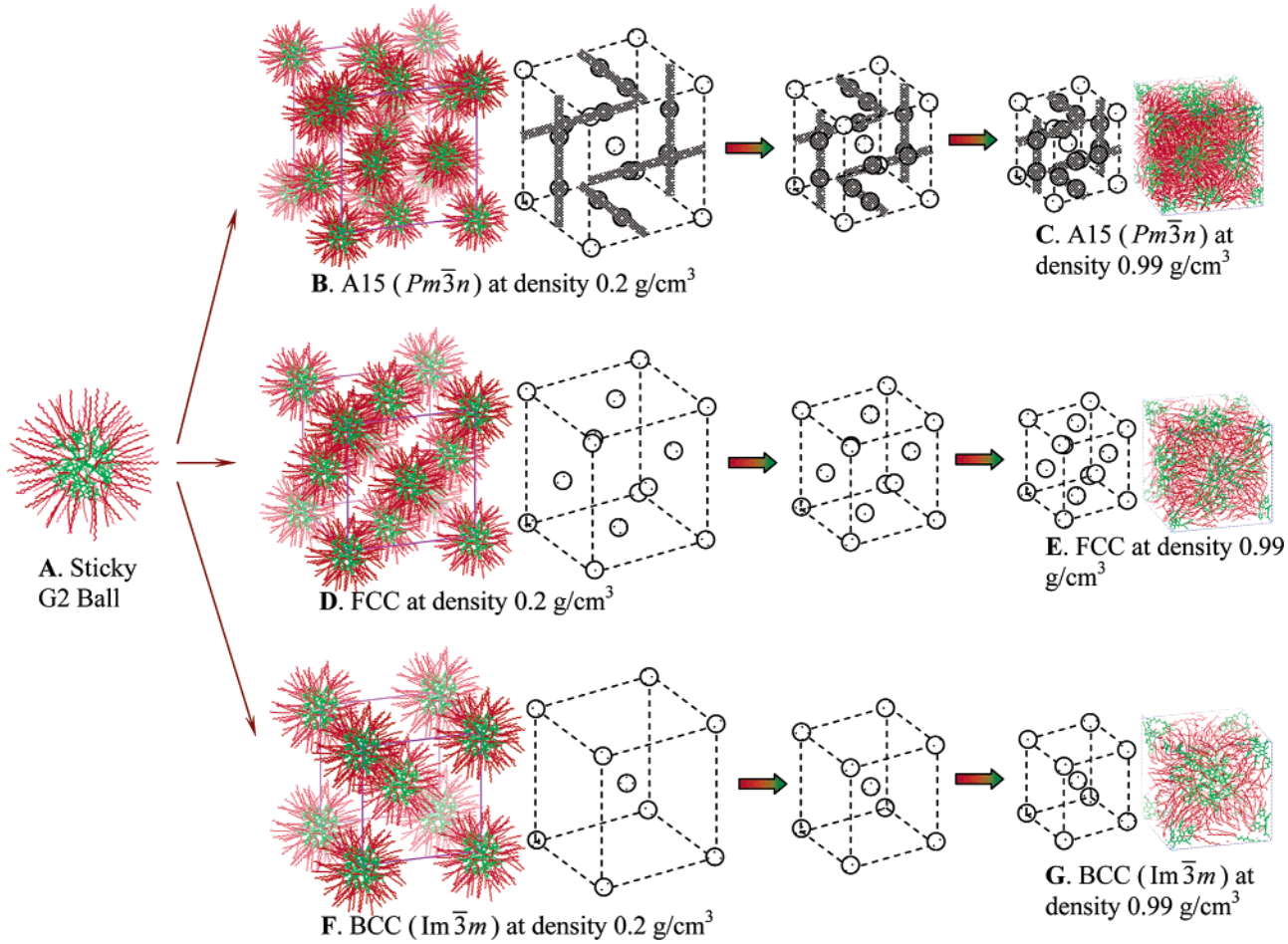

Figure 6. Packing dendrimer balls into A15, FCC, BCC at low density (0.2 g/cm^3) followed by compression in multiply small steps until the target density (0.99 g/cm^3) is achieved.

including three types of dendrimer balls: Smooth/Valentino (Figure 4a), Sticky/Einstein (Figure 4b), and Asymmetric/Punk (Figure 4c).

From the isolated dendrons of compounds G2(**I**), G3(**II**), and G4(**III**), we first constructed the Sticky/Einstein balls for G2, G3, and G4. The analysis of the experimental X-ray result

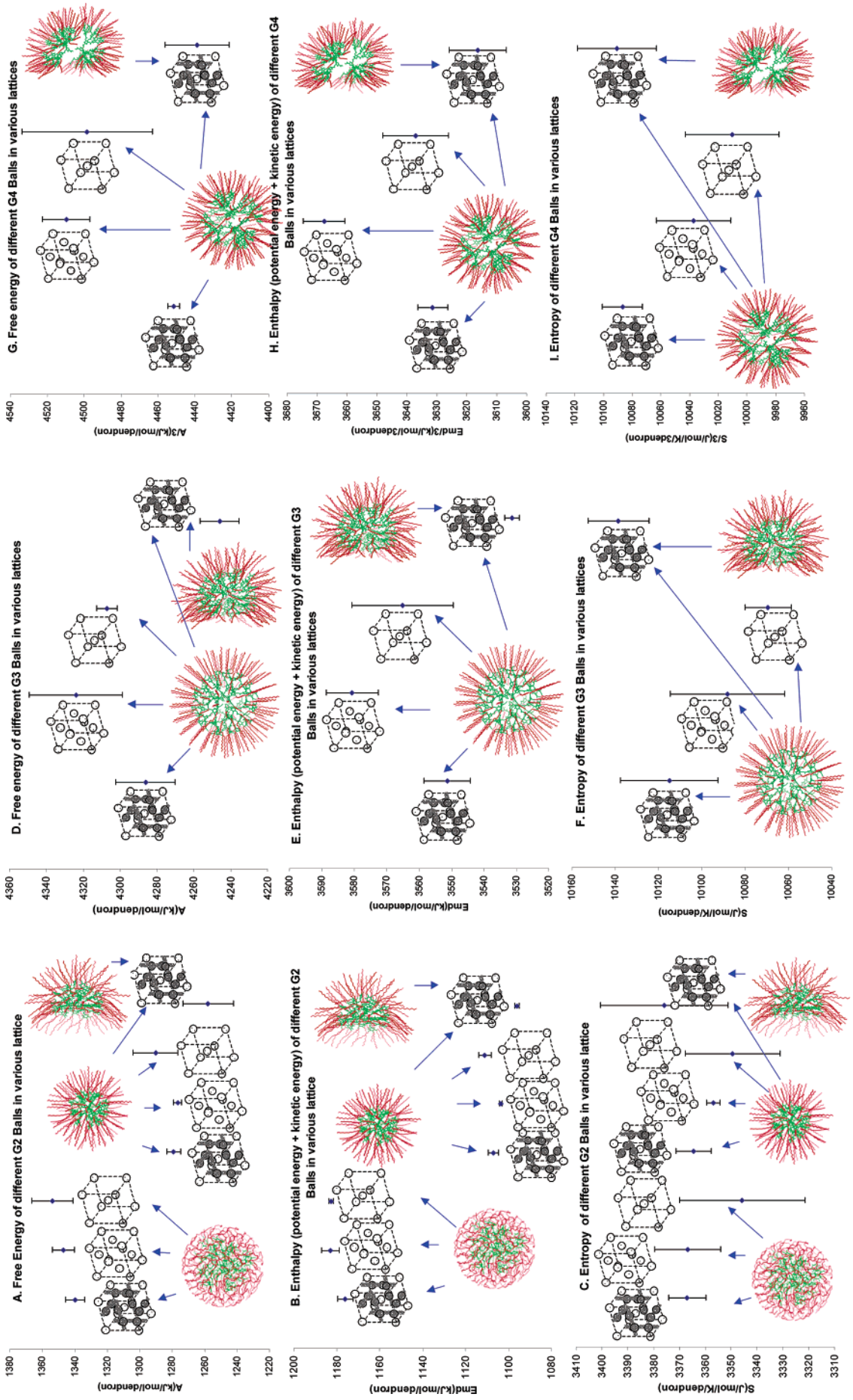

Figure 7. Helmholtz free energy ($A = E_{md} - ZPE - TS$), enthalpy (E_{md} = potential energy from MD including kinetic energy but not zero point energy), and entropy (S) of different shape balls in various lattices. Each MD simulation is carried out with a fixed volume using a Nose−Hoover thermostat (denoted as NVT) at the density 0.99 g/cm^3. These MD simulations are carried out at a temperature of 277 K, which is the recrystallization temperature in ref 16. Shown here are the average and the RMS uncertainties, obtained from three independent MD simulations using independent sets of initial velocities.

suggested that 11.3 dendrons self-assemble into the soft balls in G2, 5.8 dendrons assemble into the soft balls in G3, and 1.9 assemble to form the balls for G4 (see Table 3 of ref 16). We construct the G2, G3, and G4 balls to have 12, 6, and 2 dendrons, respectively. This leads to 108 C12 alkyl chains for G2 and 162 for both G3 and G4. Figure 5 illustrates the preparation of the G2 balls.

From the isolated G2 dendron, we first construct the "Sticky/Einstein G2 Ball" composed of 12 dendrons, with the polyethylene chains initially all-trans, pointing outward uniformly from the ball center. An energy minimization of 500 steps is then performed to optimize the structure.

Next, we constructed the structure of the "Ball Frame" shown in Figure 5. This frame is prepared using 500 C_R atoms (the type for C in aromatic assemblies including graphite) uniformly distributed on a sphere. The uniform distribution of C_R atoms is obtained by first placing a point charge on each atom and then minimizing (1000 steps) the Coulombic energy, with a constraint of keeping the C_R atoms a fixed distance from the center. The "Ball Frame" is a tool to be used to compress the "Sticky/Einstein ball" to the "Smooth/Valentino ball" by starting with a radius outside of the atoms for the sticky ball and steadily reducing the radius, forcing the alkyl chains to deform and eventually form the structure of the Smooth ball, as described next.

To select an initial radius for the "Ball Frame", we note that the surface atoms (C_33) of the "Sticky G2 Ball" lead to a RMS radius of 27.4 Å, whereas the closest distance of soft balls in various lattices (A15, BCC, and FCC) at the expected density 0.99 g/cm^3 is 34.8 Å. Thus, we started the size of the "Ball frame" at 27.4 Å + 4 Å = 31.4 Å and contracted it to 34.8 Å/2 + 4 Å = 21.4 Å in 10 steps. Here, 4 Å is the favored distance between C_R and C_33 atoms. In each step, the size of the "Ball Frame" decreases 1 Å followed by 200 steps of energy minimization on the dendrimer. The final result is the "Smooth G2 Ball" shown in Figure 5.

By rotating a line of 12 C_R atoms 36 times, we get the "Cone Frame" as shown in Figure 5. After compressing the cone angle to almost 0°, we align the "Cone Frame" together with "Sticky G2 Ball" as shown in Figure 5. We then expand the cone angle step by step followed by 200 steps of energy minimization unless there is no overlap between the two same Asymmetric/Punk balls at the distance of 34.8 Å as shown in Figure 4c.

3.3. Packing Balls into Various Lattices. From the dendrimer balls prepared in section 3.2, except for the dendrimer ball with Smooth shape, we first pack them together in various lattices (A15, FCC, BCC) at low density (0.20 g/cm^3) as shown in Figure 6B,D,F. We then shrink the unit cell steadily by 1 Å each step followed by 500 steps of minimization to allow the polyethylene chains of neighboring balls to pack together. In each step, the ball center is translated to be at the correct position for the new decreased cell length, but the structure within each ball remains unchanged. During these minimizations, we fix the acid hydrogen atoms (denoted as atom type H___A) of the carboxylic acid at the core of each dendron to retain the position of the ball center. With this procedure, we get the A15, FCC, and BCC lattices at the target density (0.99 g/cm^3) as shown in Figure 6C,E,G.

For the A15 structure, there are two crystallographically inequivalent types of positions: the face position (2 atoms per face, 6 per cube) and the corner/body center positions (one each per cube), as indicated by black circles and white circles in Figure 6. The face positions lead to the closest contacts with neighboring balls, and hence we place the anisotropic balls (Figure 4c) at these face positions. For the corner/body center positions of A15, we started with sticky balls. We denote this structure as the "Anisotropic A15" structure.

For the dendrimer ball with smooth shape, we placed the balls on the desired positions of various lattices at the target density (0.99 g/cm^3). Our preparation procedure for smooth balls (detailed in section 3.2) guaranteed that the balls would not touch each other when placed into the structures at density 0.99 g/cm^3. Thus, the initial structure for the smooth balls led to significant void volume. We then performed an energy minimization of 500 steps, followed by the molecular dynamics runs as described in section 2.3. We find that the tail chains relax to fill in the void volume that has been left in the initial structure during energy minimization and molecular dynamics.

In the MD simulations, we use eight independent dendrimer balls for A15 leading to 15 840 independent atoms per cell for G2, 24 336 for G3, and 24 528 for G4. Note that there are no hydrogen atoms in the alkyl chains as the united atom force field is used. For the FCC structure, we use four independent balls, leading to one-half the number of atoms as for A15. For the BCC structure, we use two independent balls, leading to one-fourth the number of atoms as for A15.

3.4. Free Energy of Various Lattices. Figure 7 shows the free energy (A), energy (E_{md}), and entropy (S) of different ball shapes packed into various lattices. The comparison of generations 2, 3, and 4 is shown in Figure 7ABC, DEF, and GHI, respectively.

Comparing Figure 7A with 7B, 7D with 7E, and 7G with 7H, we see that free energy of various lattices follows the same trend as the enthalpy of various lattices. The best lattice is the "Anisotropic A15" lattice for all generations (2, 3, and 4).

For generation 2, A15, FCC, and BCC composed of sticky balls are essentially not distinguishable. We have the same conclusion for A15, FCC, and BCC lattices composed of smooth G2 Balls. However, the lattices composed of sticky balls are found to be much more stable than the lattices composed of smooth balls.

From Figure 7C,F,I, we can see that the deviations in entropy are pretty big as compared with those of enthalpy in Figure 7B,E,H, which makes the difference among those lattices not distinguishable. However, we see the same trend for all generations: Anisotropic A15 > sticky A15 > sticky FCC > sticky BCC, indicating that A15 is slightly favorable in terms of entropy consideration.

For generations 3 and 4, the differences among various lattices are larger than those for generation 2. We can see that the best lattice is still Anisotropic A15 lattice, followed by A15, BCC, and FCC in that sequence.

In conclusion, Anisotropic A15 lattice gives the best (lowest free energy) packing of the G2, G3, and G4 balls composed of compounds **I**, **II**, and **III**. For the three packing mechanisms proposed in section 3.1, anisotropic packing is the best. This is

(36) Accelrys_Inc. *Cerius2 Modeling Environment, Release 4.0*; Accelrys Inc: San Diego, 1999.

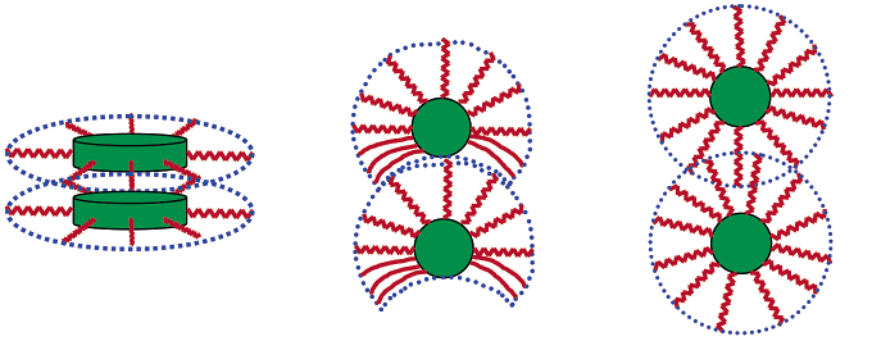

A. Disk shape composed by tapered fan shape dendron

B. Asymmetric/Punk ball shape as intermediate shape between disk shape and cone shape

C. Isotropic ball shape composed by cone shape dendron

Figure 8. Packing of disk shape, Asymmetric/Punk ball shape, and isotropic ball shape dendrimers.

because it allows a good balance between interball vdW and intraball vdW and accommodates a variety of ball−ball distances without sacrificing the all-trans intrachain conformation of the alkyl chains. In contrast, slippery packing with the smooth ball shape leads to bad enthalpy, although it has the optimal intraball vdW.

Furthermore, the Asymmetric/Punk ball shape can be viewed as the intermediate between the disk shape and isotropic ball shape as shown in Figure 8. Dendrons with a tapered fan shape assemble flat pizza-like slices into disks, which then stack into columns that eventually form a hexagonal array.[15] Dendrons with more alkyl chains are cone-shaped and assemble into supramolecular spheres. So far, these spherical aggregates have been known to pack on three lattices, Cub $Pm\bar{3}n$,[16] Cub $Im\bar{3}m$,[17] and Tet $P4_2/mnm$.[1] By tuning the number of alkyl chains, there exists the intermediate shape between the disk shape and isotropic ball shape as shown in Figure 8B. In fact, from the analysis in Figure 7, this type of Asymmetric/Punk ball shape makes the A15 structure superior to other structures.

For a specified compound,[1] experiments find the following phase sequences at different temperatures: glass < 110 °C < Col_h (Col_h = hexagonal columnar) < 140 °C < Cub $Pm\bar{3}n$ < 153 °C < Tet $P4_2/mnm$ (tetragonal distortion of cubic packing) < 163 °C < Iso (isotropic liquid).

This indicates that the dendron exhibits a tapered fan shape at low temperature, while it adopts a cone shape at high temperature. In other words, the packing of disk-shaped dendrimers in Figure 8A is enthalpically preferred and the packing of ball-shaped dendrimers in Figure 8C is entropically favored. The results for the Asymmetric/Punk ball shape in Figure 8B suggest a way to understand the above phase sequence. The Col_h structure is composed of 100% disks as shown in Figure 8A. The Cub $Pm\bar{3}n$ structure has 75%(6/8) Asymmetric/Punk balls (coordination number 14) and 25%(2/8) isotropic balls (coordination number 12). The Tet $P4_2/mnm$ structure has 67%(20/30) Asymmetric/ Punk balls (16 of them have coordination number 14 and 4 of them have coordination number 15) and 33%(10/30) isotropic balls (coordination number 12).[1] Our assumption that tapered fans are favored enthalpically is consistent with the observed ordering of the phases with Col_h lowest, Cub $Pm\bar{3}n$ next, and Tet $P4_2/mnm$ at the highest temperature.

In the Cub $Pm\bar{3}n$ liquid crystal phase formed by compounds G2(**I**), G3(**II**), and G4(**III**), it is found that a nearly integer number of dendrons self-assemble into a sphere. Specifically, the packing numbers of dendrons in each sphere of G2, G3, and G4 are 11.3, 5.9, and 1.9.[16] We use integer numbers 12, 6, and 2 in the simulation. When an isolated ball formed by aggregation of dendrons is considered, the core part of the ball is compact involving interactions between the phenyl groups. However, the soft corona, which is composed of polyethylene chains, is quite loose. Thus, the packing number of dendrons into a ball is determined by the core part of the dendrimer ball. The average radius gyrations of the core part of the G2, G3, G4 balls from our best Anisotropic A15 structure (equilibrated after 60 ps dynamics) are 11.02, 13.39, and 13.88 Å, respectively. Assuming that the density is uniform in the ball core part, we derive the volume occupied by the core from the relation of $Rg = \sqrt{3/5}r$. Dividing this core volume by the volume of the phenyl group of each dendron at density 0.99 g/cm^3, we get the maximum packing number of dendrons in each G2, G3, and G4 ball: 12.48, 7.15, and 2.62. This result indicates that the packing of dendrons into a ball is not yet saturated. The "anisotropic packing" as shown in Figure 4C results in the nonspherical balls and unsaturated packing. Table 2 lists the physical properties of the dendrimer balls formed by 12G2-AG, 12G3-AG, and 12G4-AG.

Figure 9 shows the density of states (power spectrums) of various G2 lattices, which includes the Anisotropic A15 lattice and FCC, BCC lattices composed of the sticky shape G2 balls. Other lattices, which are not shown here, have similar power spectrums. From Figure 9, we can see that the power spectra of various lattices are almost indistinguishable, even in the zoom-in of Figure 9B. Indeed, the analysis of Figure 7 shows that there is no significant difference in the entropies of various structures.

3.5. Comparison with Experimental X-ray. Figure 10 shows the X-ray intensities of 12G2-AG, 12G3-AG from experiment[16] and prediction from the best "Anisotropic A15 structure". The predicted intensities fit the experimental intensities very well. This confirms our predicted structure, free energy analysis here, and the electron density profile analysis in ref 16.

3.6. Free Energy Profile over Density of Various Lattices. To understand the packing process of the soft balls, we calculate

Table 2. Physical Properties of the Spherical Supramolecule Formed by 12Gn-AG

generation	μ(model)[a]	N(model)[b]	Rg/Å[c]	Rg(core)/Å[c,d]	μ(predicted)[e]	μ(exptl)[f]	saturation degree[g]
2	12	4680	17.75	11.02	12.48	11.3	90.5%
3	6	7092	20.24	13.39	7.15	5.8	81.1%
4	2	7116	20.97	13.88	2.62	1.9	72.5%

[a] We use 12, 6, and 2 dendrons to form the dendrimer ball of generation 2, 3, and 4, which are close to the experimental values of 11.3, 5.8, 1.9.[16] [b] There are a total of 4680, 7092, and 7116 atoms in each dendrimer ball of 12G2-AG, 12G3-AG, and 12G4-AG constructed for simulation. However, the hydrogen atoms in the $C_{12}H_{25}$ tail chains are implicit during molecular dynamics (see section 2.1). [c] The radius gyration of each ball or core of the ball is evaluated from the best liquid crystal structure at density 0.99 g/cm^3 after 60 ps NVT molecular dynamics and averaged from the eight independent balls in the unit cell. [d] This is the radius gyration of the core part of each ball (excludes the $C_{12}H_{25}$ tail chains). [e] On the basis of the relation of $Rg = \sqrt{3/5}r$, we determine the volume occupied by the core part of each ball from *Rg*(core). We then divide it by the volume of the core part of each dendron at the density 0.99 g/cm^3, and we get the maximum packing number of dendrons in each G2, G3, and G4 ball. [f] This packing number was determined from X-ray analysis and listed in Table 3 of ref 16. [g] Saturation degree is defined as μ(exptl)/μ(predicted).

the free energy, enthalpy, and entropy of various lattices at different densities as shown in Figure 11. The structures are prepared as described in section 3.3 and Figure 6. For the densities lower than 0.99 g/cm^3, we fix the central atom H___A in the core of each dendron to keep the ball centers at the desired positions in the lattice during molecular dynamics.

From Figure 11B, we can see that the enthalpies of various lattices all have a minimum at ~0.99 g/cm^3. The best structure AA15 (Anisotropic A15) is only favored at a density above 0.90 g/cm^3. The enthalpy decreases monotonically during the packing process. The interball vdW interaction dominates the packing energy. It decreases slowly in the early packing stage due to less interaction among the soft balls at low density.

The entropies for all structures decrease with increasing density, as shown in Figure 11C. That is because the overlap between the neighboring soft balls constrains the conformations of the chains of the balls, leading to a short-ranged repulsive interaction. The differences among various lattices are negligible above a density of 0.6 g/cm^3. However, entropy evaluation has a big deviation at low density as shown in Figure 11C. For nearly isolated soft balls at low density, there is much more flexibility, leading to the large differences.

The free energy profiles are shown in Figure 11A. The free energy profiles of various lattices show the same trend, which can be approximately described as three levels. The lowest level is at the density from 0.2−0.3 g/cm^3. From 0.5−0.99 g/cm^3, the free energy shows a flat stage profile as the middle level. The free energy is the worst (highest) at the high density, 1.10 g/cm^3.

The free energy profile over volume of the best Anisotropic A15 lattice at 277 K as shown in Figure 12 indicates two stable phases: (a) a condensed phase at the density 0.99 g/cm^3; and (b) an isolated micelle phase at the density 0.30 g/cm^3. This figure is derived from Figure 11A and essentially is an A−V plot of the micelle from the condensed phase to the isolated phase. The isolated phase is evaluated in a vacuum without solvent and is unphysical. The critical pressure determined from the two stable phases is 0.033 GPa, which is bigger than 1 atm. This implies that in the recrystallization process, the unfavorable solvent at 277 K is the driving force to form the condensed phase.

In the BCC and FCC lattices, the ball interacts equally with its neighbors. Thus, we can derive a two-body potential from Figure 11. Figure 13 shows the two-body free energy/enthalpy potential in BCC and FCC lattices. Obviously, the two-body potential of the soft dendrimer balls is lattice dependent. The reason is that the soft dendrimer balls self-adjust its shape and interaction in different lattices. However, the two-body potential from BCC and FCC lattices shares the same trend. The two-body free energy potential in BCC and FCC lattices can be explained as a so-called "square shoulder potential".[37−40] In this potential, the soft balls do not interact with each other when they are far apart, and they interact via a constant repulsive value at short distance. This soft shoulder arises from the entropy repulsive interaction. The shoulder positions in BCC and FCC are different due to the different neighbor distribution.

The two-body E_{md} (enthalpy) potentials in BCC and FCC are similar to the Lennard-Jones potential. Also, the optimum distances in BCC and FCC are different (see Figure 13B). From the optimum point (at the density 0.99 g/cm^3), we can derive the Lennard-Jones 12 6 potentials as shown in Figure 13B (solid points). The two-body enthalpy potential of soft dendrimer balls has a much sharper well than the Lennard-Jones potential. The interaction of the soft balls increases dramatically when bringing them together.

3.7. Packing Efficiency of Ideal Soft Balls (Which Overlap Each Other) and Some General Discussions. To investigate the geometric difference of various lattices in the packing of soft balls, we use the A15, FCC, and BCC lattice boxes of generation 2 above (at the same density: 0.99 g/cm^3) and put ideal balls into desired positions. By increasing the ball radius and letting the balls overlap each other, the void volume in the lattice decreases as shown in Figure 14 (from numerical results).

When the ball is small enough and there is no overlap between balls, A15, FCC, and BCC give the same void volume. By increasing the ball size from 18 to 21 Å, the balls in A15 overlap first, then BCC, followed by FCC. That is because FCC is the closest packing lattice for hard balls. In the range of 18−21 Å, FCC has the least void volume. However, if we increase the ball size from 21 to 25 Å, FCC shows the biggest void volume. BCC has the least void volume, but A15 is comparable. Further increasing the soft ball size fills all of the space , and the void volume is zero for all lattices.

The least void volume means the soft balls use the space in the most efficient way and the overlap between the balls has been kept to a minimum. Considering the entropy repulsive interaction between the soft balls discussed in section 3.6, we conclude that the less overlap in the lattice, the better the free energy. In view of this, FCC is the lest efficient lattice for the ideal soft ball, while BCC is the most efficient lattice.

From the analysis in the previous sections, we can see that dendrimer balls are not ideal soft balls, which can self-adjust their shape anisotropically to get the best packing of the soft corona. Indeed, they adopt the intermediate shape between the disk and isotropic ball to achieve a balance between enthalpy and entropy, and they assemble into the A15 lattice.

(37) Blohuis, P.; Frenkel, D. *J. Phys. C* **1997**, *9*, 381.
(38) Rascon, C.; Velasco, E.; Mederos, L.; Navascues, G. *J. Chem. Phys.* **1997**, *106*, 6689.
(39) Lang, A.; Kahl, G.; Likos, C. N.; Lowen, H.; Watzlawek, M. *J. Phys. C* **1999**, *11*, 10143.
(40) Velasco, E.; Mederos, L.; Navascues, G.; Hemmer, P. C.; Stell, G. *Phys. Rev. Lett.* **2000**, *85*, 122.

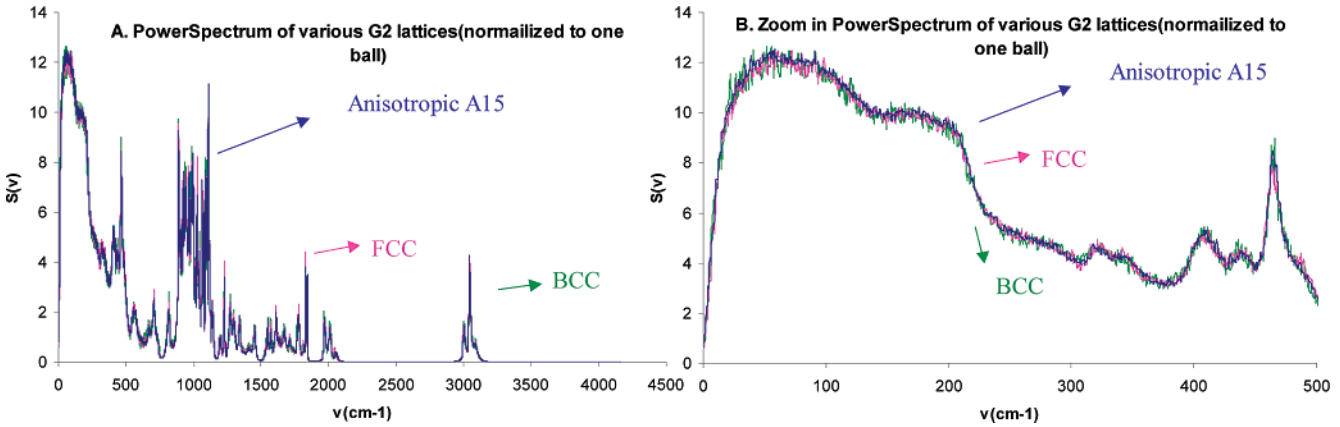

Figure 9. Power spectrum of various G2 structures using the best case for each structure (symmetric sticky balls for FCC and BCC, and asymmetric sticky balls for A15). Each power spectrum is from one of the three MD runs. There results are normalized to one ball; separate colors (blue for A15, purple for FCC, and green for BCC) are used for various structures, but the differences are negligible.

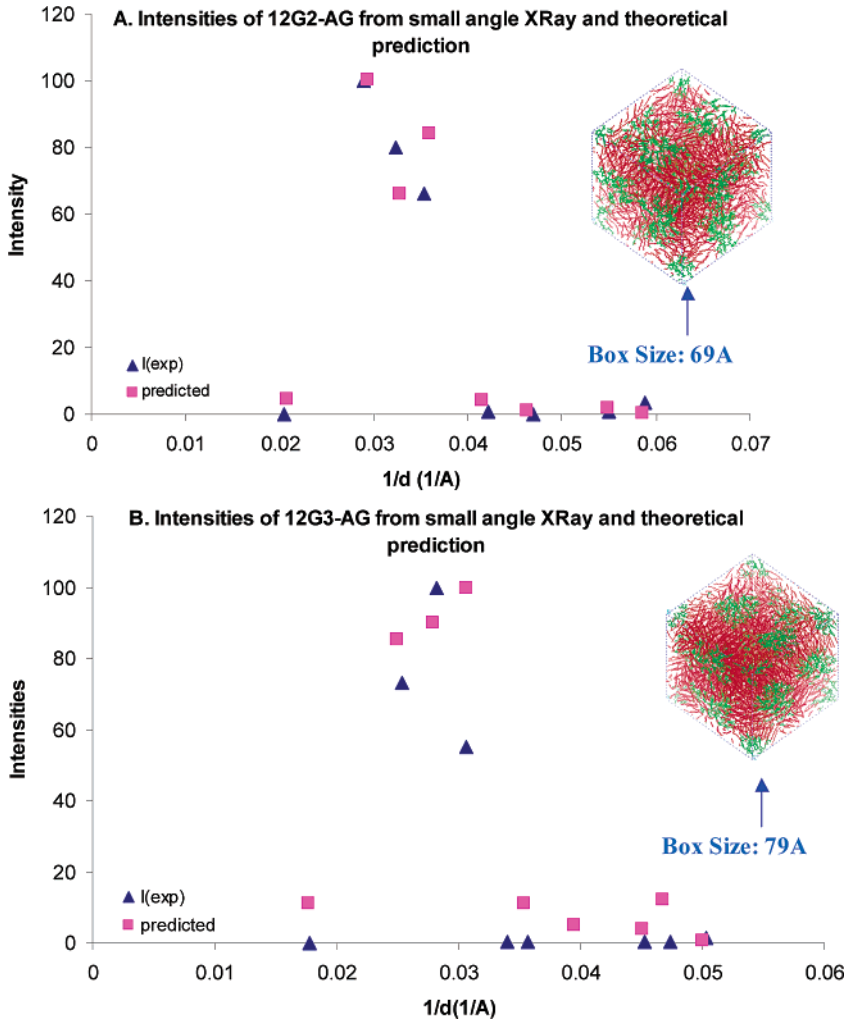

Figure 10. Predicted X-ray intensities of 12G2-AG, 12G3-AG dendrimers from the best structure, Anisotropic A15 structure, as compared with experiment.[16] The X-ray diffraction intensities are calculated using the "Diffraction-Crystal" module in Cerius2 4.0. No polarization factor, crystal monochromator factor, or temperature factor is applied to the intensity calculations. These intensities are from a single snapshot from the MD trajectory (after 60 ps). We apply the factor 0.98 to the predicted intensities of 12G2-AG, which arises from power (11.3/12, 1/3); where experiment has 11.3 dendrons, our structure has 12 dendrons in each ball. The hydrogen atoms of polyethylene chains are not considered during the intensity calculations.

Kamien et al.[41] analyzed the stability of different lattices (A15, BCC, FCC) by considering the tension in the *AB* interface of a diblock copolymer and the stretching of the polymers. They concluded that the BCC lattice minimizes the stretching part and the A15 lattice minimizes the tension in the interface. They argued that the A15 lattice should be favored as the blocks become more symmetric and corroborated this through SCFT.

(41) Grason, G. M.; Didonna, B. A.; Kamien, R. D. *Phys. Rev. Lett.* **2003**, *91*, art. no. 058304.

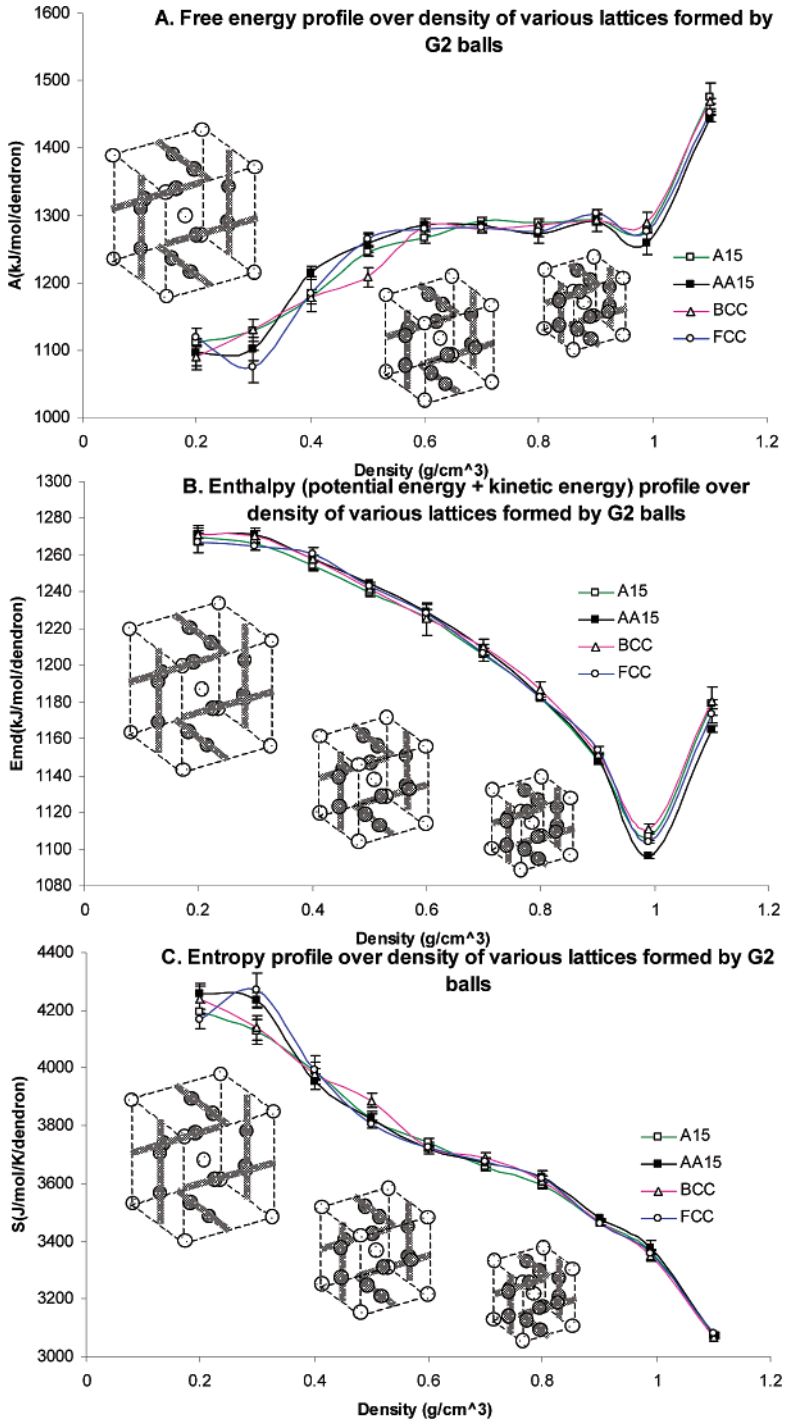

Figure 11. Free energy, enthalpy, and entropy as a function of density for four cases of G2 dendrimers. AA15 is the A15 structure composed of anisotropic balls on the face and isotropic balls on the corner and body center. The other three structures, A15, FCC, and BCC, are based on isotropic balls only. MD simulation details are the same as in Figure 7.

Indeed, they argued that the BCC lattice minimizes the stretching of the polymers, which is consistent with our analysis. We concluded that there exists an entropic repulsive interaction between soft balls and the BCC lattice minimizes it in terms of ideal soft balls. From an analysis of the competition between enthalpic and entropic interactions in soft balls, we find that the stretching of the polymers (deformation from the sphere cell to the Voronoi/Wigner-Seitz cell) arises from the entropic effects.

However, the tension in the *AB* interface analyzed by them might not be directly applicable to the dendrimer liquid crystal system we studied here. The authors claimed that when the volume fraction of *A*-type monomers (ϕ) is large enough, the *AB* interface takes on the shape of the Voronoi cell. On the basis of that, they concluded that A15 minimizes the interfacial tension.

We consider that the packing mechanism of the polyethylene segments of the corona of the soft ball, but not the interfacial tension between the aromatic phase and aliphatic phase, is the key factor in determining the efficiency of various lattices. Indeed, Percec's group found that the density of the polyethylene segments could be used to tune the phase of the dendrimer liquid

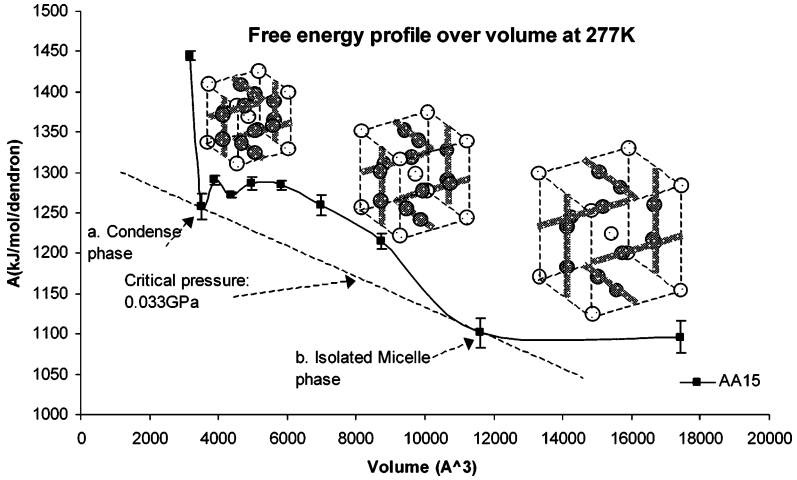

Figure 12. Free energy profile over volume of Anisotropic A15 lattice at 277 K.

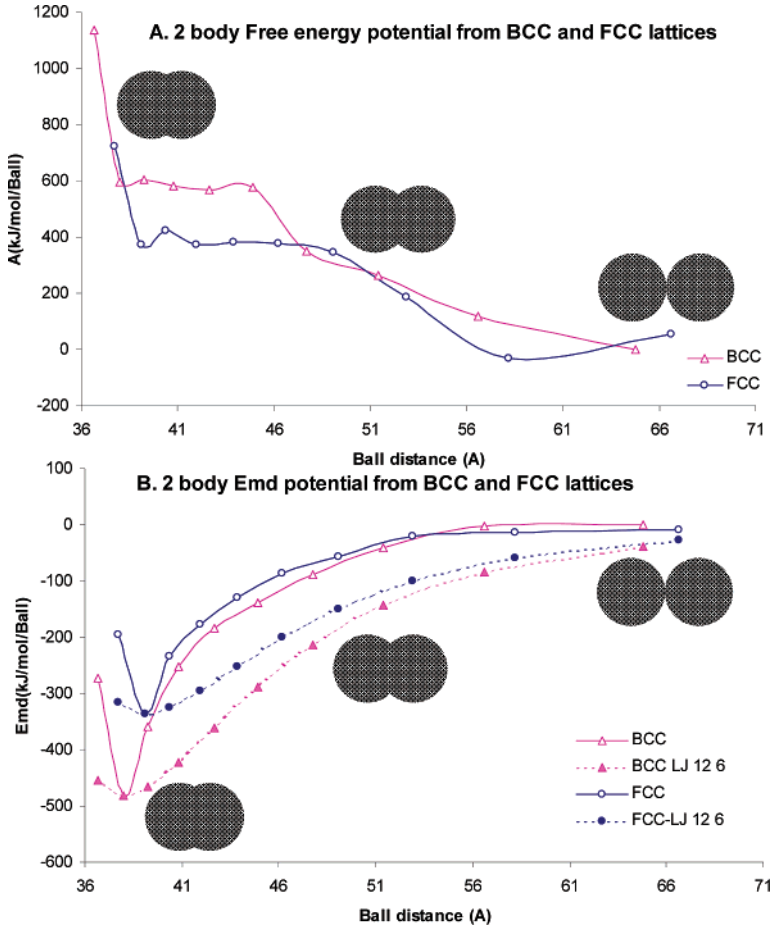

Figure 13. Two-body potential from BCC and FCC lattices.

crystal. Our simulation results indicate that the dimmer balls on the face of A15 structure prefer a nonspherical shape, leading to a good packing of the polyethylene segments. We believe that the interfacial tension is less important between the aromatic phase and the aliphatic phase, although it might be crucial for the diblock copolymer phases.

Kamien's group also proposed some guidelines for considering the principle of packing colloids.[42,43] They simplified the aliphatic phase in the dendrimer liquid crystal as a dodecyl bilayer, which is dominated by a repulsive free energy that scales as the inverse of the layer thickness, d^{-1}. They argued that A15 is the most stable structure because the entropy is maximized through the minimization of the interfacial area in the bilayer.

We consider the dendrimer liquid crystals to be different from colloidal crystals, which contain solvent. The interaction among colloidal micelles will always be repulsive, even in the crystal. However, in the dendrimer liquid crystal, where there is no

(42) Ziherl, P.; Kamien, R. D. *Phys. Rev. Lett.* **2000**, *85*, 3528.

(43) Ziherl, P.; Kamien, R. D. *J. Phys. Chem. B* **2001**, *105*, 10147.

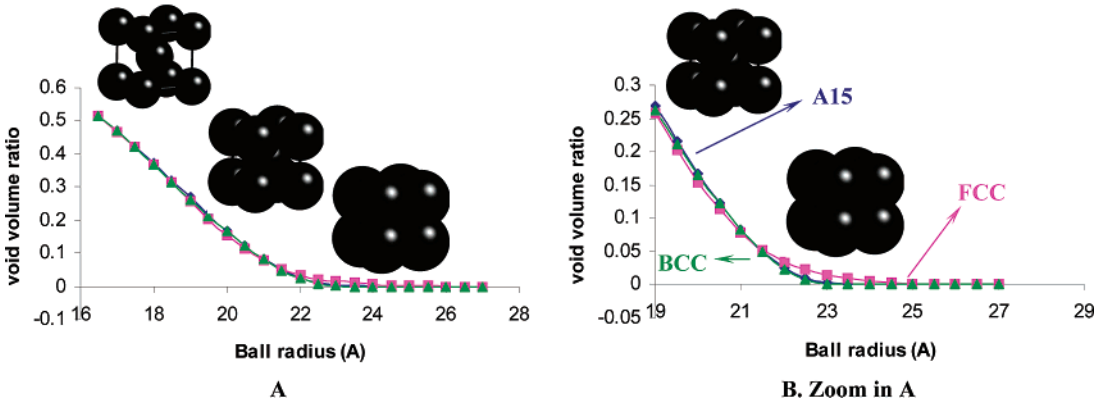

Figure 14. Packing efficiency of ideal soft balls (which overlap each other). The curves are obtained from numerical results.

solvent, the aliphatic segments of the neighboring balls can pack each other favorably.

Furthermore, we consider that the bilayer approximation may not be accurate enough to distinguish various lattices. Our atomistic simulation results indicate that the various lattices formed by the same type of dendrimer balls are not distinguishable in terms of free energy (e.g., Figure 7A).

4. Conclusions

Self-assembled supramolecular organic liquid crystal structures at nanoscale have potential applications in molecular electronics, photonics, and porous nanomaterials. Most of them are aggregated by soft spheres, which have soft coronas and overlap each other in the packing process.

On the basis of our simulations on the atomistic scale, we propose three packing mechanisms of soft balls, "Sticky packing", "Slippery packing", and "Anisotropic packing", and we use the vibrational density of state (DoS) derived from classical molecular dynamic simulations to investigate the efficiency of various lattices for soft balls from simulation.

By focusing on the three compounds reported by Percec et al. (*J. Am. Chem. Soc.* **1997**, *119*, 1539), which form spheres with a nearly integer number of dendrons, we compare the efficiency of various lattices and different packing methods. For the soft spheres with aliphatic coronas composed of polyethylene chains, "Sticky packing" is better than "Slippery packing". Anisotropic packed A15 is favored over FCC, BCC lattices. Predicted X-ray intensities of the best structures fit the experiments very well.

"Anisotropic ball packing" proposed here plays an intermediate role between the enthalpy-favored "disk packing" and entropy-favored "isotropic ball packing", which explains the phase transitions at different temperatures.

Free energy profiles over the density of various lattices are essentially the same, which indicates that the preferred lattice is not determined during the packing process. Both enthalpy and entropy decrease as the density increases. The free energy profile over volume shows two stable phases: the condensed phase and the isolated micelle phase. The two-body potential of the soft dendrimer ball is lattice dependent, because it self-adjusts its shape and interaction in different lattices. The shape of the free energy potential is similar to that of the "square shoulder potential".

A model explaining the packing efficiency of ideal soft balls in various lattices is proposed in terms of geometrical consideration. BCC has the least void volume for the ideal soft ball, while FCC has the biggest.

Acknowledgment. This paper is dedicated to the late Paul Miklis, who initiated the study of these Percec systems shortly after the first publication. In addition to the early stimulation by Paul, we also thank Dr. Tahir Cagin and Virgil Percec for many helpful discussions about these dendrimers, and we thank Dr. Mario Blanco with help using Lammps. This research is based in part on work supported by the U.S. Army Research Laboratory and the U.S. Army Research Office under grant number DAAG55-97-1-0126 (MURI-program officer Doug Kiserow). The facilities of the MSC used in this research have been supported by grants from the ARO (DURIP), ONR (DURIP), NSF (MRI), and IBM (SUR). Other support to the MSC is provided by the NIH, NSF, DOE, Chevron-Texaco, General Motors, Seiko Epson, Asahi Kasei, Beckman Institute, and Toray Corp.

JA038617E